

Effect of inhomogeneities on backward and forward Brillouin scattering in photonic crystal fibers

Birgit Stiller^a, Michaël Delqué^a, Min W. Lee^a, Stella Foaleng Mafang^b, Jean-Charles Beugnot^b, Alexandre Kudlinski^c, Luc Thévenaz^b, Hervé Maillotte^a and Thibaut Sylvestre^a

^aDépartement d'Optique, Institut FEMTO-ST, Université de Franche-Comté, Besançon, France;

^bGroup for Fibre Optics, Institute of Electrical Engineering, EPFL Lausanne, Switzerland;

^cLaboratoire de Physique des Lasers Atomes et Molécules, IRCICA Lille, France

ABSTRACT

Photonic Crystal Fibers (PCF) play a crucial role for fundamental investigations such as acousto-optical interactions as well as for applications, such as distributed sensors. One limiting factor for these experiments is the fiber inhomogeneity owing to the drawing process. In this paper we study the effect of structural irregularities on both the backward and forward Brillouin scattering by comparing two PCFs drawn with different parameters, in order to minimize diameter fluctuations. We fully characterize their Brillouin properties including the backward Brillouin spectrum, the Brillouin threshold, a distributed measurement along the fibers and polarized Guided Acoustic Wave Brillouin Scattering (GAWBS). In the Brillouin spectrum we observe a single peak as in a single-mode fiber whereas former investigations have often shown a multiple peak spectrum in PCFs with small core. The theoretical and experimental values for the Brillouin threshold are in good agreement, which results from the single peak spectrum. By using a Brillouin echoes distributed sensing system (BEDS), we also investigate the Brillouin spectrum along the fiber with a high spatial resolution of 30 cm. Our results reveal a clear-cut difference between the distributed measurements in the two fibers and confirm the previous experiments. In the same way the GAWBS allows us to estimate the uniformity of the fibers. The spectra show a main peak at about 750 MHz, in accordance with theoretical simulations of the acoustic mode and of the elasto-optical coefficient. The fiber inhomogeneity impacts on the stability and the quality factor of the measured GAWBS spectra. We finally show that the peak frequency of the trapped acoustic mode is more related to the optical effective area rather than the core diameter of the PCF. Thus measuring the main GAWBS peak can be applied for the precise measurement of the effective area of PCFs.

Keywords: Brillouin scattering, distributed sensing, photonic crystal fibers

1. INTRODUCTION

Brillouin Scattering in optical fibers results from the interaction between light and acoustic waves through electrostriction.¹ The Brillouin gain and the Brillouin frequency shift (BFS) mainly depend on the overlap of these waves in the fiber core and on the material. At the same time temperature and strain influence the velocity of the acoustic wave and thus the BFS. Since the acoustic modes are sensitive to temperature and strain, Brillouin backscattering can be used for distributed sensing. This was investigated in single mode fibers (SMF)² as well as in photonic crystal fibers (PCF).³ Due to their high nonlinearity and their higher Brillouin gain PCFs have received particular attention for temperature and strain sensing. It has recently been reported that PCF with small core exhibit in most cases a multi-peak Brillouin spectrum due to the periodic air-hole microstructure.⁴⁻⁶ This behavior could be advantageously used for simultaneous strain and temperature distributed measurements but when multi Brillouin peaks overlap the spectra broaden and the data analysis gets more difficult. Another aspect that limits distributed measurements is the inhomogeneity along the fiber which has an influence on the BFS and consequently on the temperature or strain measurement. This plays a crucial role for PCF since the drawing process is more delicate than for SMF. However, the inhomogeneity in PCFs has not been investigated to

Contact e-mail: birgit.stiller@femto-st.fr

the best of our knowledge. In this work we fully characterize two PCFs with nearly same air-hole microstructure but drawn with different parameters in order to minimize diameter fluctuations. The experiments presented in this work are threefold: we first perform integrated measurement of the backward Brillouin gain and threshold, then the guided acoustic wave Brillouin scattering (GAWBS) spectrum measurement, and finally the distributed measurement of the backward Brillouin gain along the fiber. Our results show that these two fibers exhibit one single peak only in the Brillouin spectrum like in a SMF and that their Brillouin threshold are in rather good agreement with classical theory. The impact of structural irregularities and strain on the Brillouin frequency shift is also clearly evidenced. We observe in particular long scale and short scale fluctuations in the BFS. We further show that it is possible to extract the effective refractive index all along the fiber from the distributed BFS measurements, which allows a quantitative estimation of fiber irregularities. With these measurements we are able to draw conclusions about the homogeneity of fibers induced by the drawing process.

The two PCFs under study have a hexagonal hole structure and their cross-sections are shown in Fig. 1. The core diameters are 5.4 μm (fiber #1) and 5.5 μm (fiber #2) respectively. They origin from the same preform but the drawing process of fiber #2 was much more controlled to obtain a greater homogeneity. Both fibers are designed to get a zero-dispersion-wavelength at 1064 nm and have an attenuation of about 8 dB/km at 1.5 μm . Further specifications such as the Group Velocity Dispersion (GVD) and the nonlinear Kerr-coefficient γ are shown as a function of wavelength in Fig. 1(c) for #2, but they are similar to those for #1. In table 1 the size of the holes, the pitch and the fiber length are listed, based on Scanning Electron Microscopy (SEM) images.

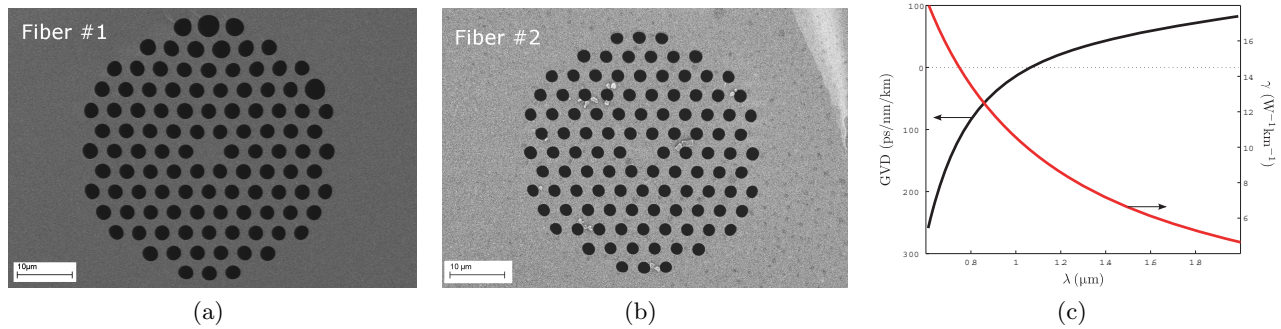


Figure 1. (a),(b) SEM images of fiber #1 and #2. (c) Group velocity dispersion and nonlinear coefficient of fiber #2

Table 1. Details of microstructure

	#1	#2
Core diameter	5.4 μm	5.5 μm
Hole diameter	2.4 μm	2.2 μm
Pitch	4.0 μm	4.0 μm
Fiber length	100 m	400 m

2. INTEGRATED MEASUREMENT

Our experiments include the distributed analysis of the Brillouin gain spectrum along the fibers with a pulsed pump as well as the investigation of Brillouin scattering with a continuous wave pump. Since in the latter case the scattered light is affected by all inhomogeneities, strain, differences of temperature or material fluctuations along its way through the fiber, it is called integrated measurement. Indeed it is an averaged image of the Brillouin spectrum integrated over the whole length of the fiber. In the integrated measurement the Brillouin backscattered spectrum, the Brillouin threshold and guided acoustic wave Brillouin scattering (GAWBS) are studied.

2.1 Backscattered Brillouin gain spectrum

The interaction between the optical pump and longitudinal acoustic waves leads to backscattered Stokes waves at the fiber input with a frequency shift:⁷

$$\nu_B = \frac{2n_{\text{eff}}V_L}{\lambda_P} \quad (1)$$

For a silica fiber with a refractive index of $n_{\text{eff}} \approx n = 1.444^8$ and an acoustic velocity of $V_L = 5960$ m/s (longitudinal) the frequency of the Stokes wave is shifted by $\nu_B = 11.1$ GHz at $\lambda_P = 1.55$ μm pump wavelength. The Stokes wave of Brillouin backscattering is characterized by a Lorentzian gain spectrum in the spontaneous regime:^{7,9}

$$g_B(\nu) = \frac{(\Delta\nu_B/2)^2}{(\nu - \nu_B)^2 + (\Delta\nu_B/2)^2} g_B \quad (2)$$

with $\Delta\nu_B$ the full width at half maximum (FWHM) of the Brillouin spectrum and the Brillouin peak gain g_B . The configuration to measure the backscattered Brillouin spectrum⁶ is depicted in Fig. 2(a). The distributed feedback laser (DFB) signal at 1550 nm is amplified by an erbium-doped amplifier and injected into an isolator and a 5 nm-filter. The light passes through an optical circulator and enters the PCF whose other end is dipped in a liquid with the same refractive index as that effects Fresnel reflections. A 50:50-coupler enables a heterodyne detection using the Brillouin signal, backscattered from the PCFs and the original laser signal. In this way we get a more accurate measurement. The resulting superposition is acquired by a 25 GHz - photodiode and amplified electrically. The insertion loss of the fibers is 1.2-1.5 dB.

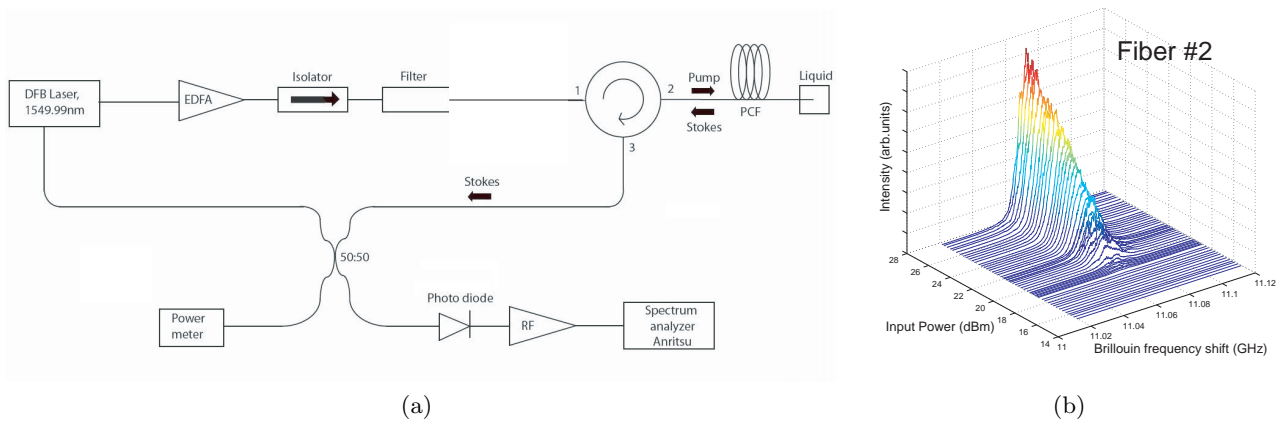


Figure 2. (a) Brillouin spectrum experimental setup:⁶ DFB Laser: distributed feedback laser; EDFA: Erbium doped fiber amplifier; PCF: photonic crystal fiber; RF: electrical amplifier, (b) Brillouin spectrum with increasing input power, fiber #2

The Brillouin spectrum obtained from fiber #2 is shown in Fig. 2(b). The Brillouin gain increases and the spectra become narrower as increasing the input power. Figures 3(a) and 3(b) show the Brillouin spectra of both fibers and one can see that there exists one single peak as in a SMF although an asymmetry in the peaks can be noticed.

In Fig. 4 we can see the FWHM depending on the input power in dBm. As reported in previous work,⁶ there is a plateau in the region of low power, i.e. in the spontaneous scattering regime. In the stimulated regime the Brillouin spectrum narrows as expected and tends to 10 MHz.¹⁰ For spontaneous scattering we assume the FWHM to be about 60 MHz for fiber #2 and 55 MHz for fiber #1 keeping in mind that the measurement is rather noisy in this part. In a SMF the FWHM is about 27 MHz which is lower as our measured ones.^{9,11} The broadening of the spontaneous Brillouin spectrum in PCF is in good accordance to former results.⁶ The FWHM in the spontaneous regime of Brillouin Scattering is inversely proportional to the phonon lifetime of the material: $\tau = \frac{1}{\pi\Delta\nu_B}$. With a FWHM of 27 MHz the natural phonon lifetime in silica is 11.7 ns which means that the amplitude of the acoustic wave decreases to 1/e in this time. Our measurements of the FWHM reveal a lifetime of 5.3 ns for fiber #2 and 5.8 ns for fiber #1. Although our PCFs are made of silica, their phonon

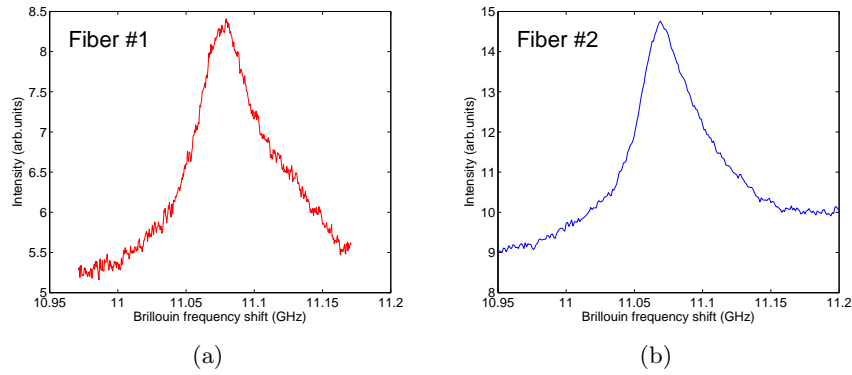


Figure 3. (a),(b) Brillouin spectrum at 11dBm of fiber #1 and #2 respectively which corresponds to spontaneous Brillouin scattering under the Brillouin threshold

lifetimes are lower than that in silica. The reason for a lower value is that the interaction of several acoustic modes at the same time causes a faster damping than with a single acoustic wave. With the measured FWHM

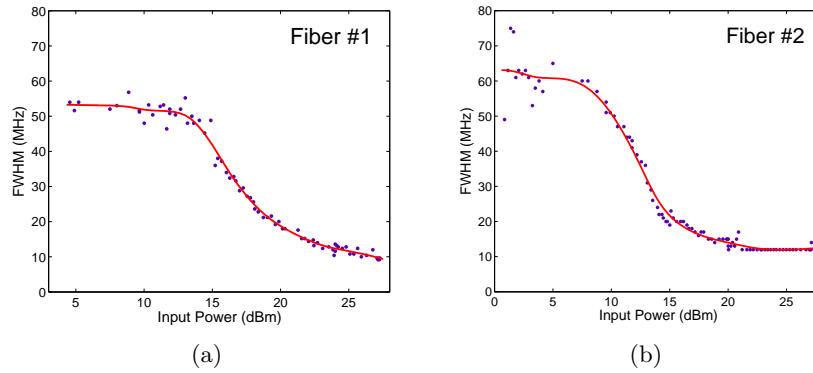


Figure 4. (a),(b) FWHM of fiber #1 and #2 for increasing input power respectively

we are also able to calculate the Brillouin gain factor g_B at frequency $\nu = \nu_B$ which reads:

$$g_B = \frac{2\pi n^7 p_{12}^2}{c\lambda_P^2 \rho_0 \nu_A \Delta\nu_B} \quad (3)$$

with p_{12} the electrostrictive constant and ρ_0 the density. In our case, assuming the FWHM to be 60 MHz (#2) and 55 MHz (#1), $g_B = 1.15 \cdot 10^{-11}$ m/W (#2) and $g_B = 1.25 \cdot 10^{-11}$ m/W (#1) respectively, using the values in table 2.

Table 2. Values to calculate the Brillouin gain

Refractive index silica	$n = 1.44$
Electrostrictive constant SMF	$p_{12} = 0.285$
Density	$\rho_0 = 2.21 \cdot 10^3 \text{ kg/m}^2$
Pump wave	$\lambda_P = 1.55 \text{ }\mu\text{m}$
Acoustic velocity	$\nu_A = 5960 \text{ m/s}$
FWHM	$\Delta\nu_B = 55 \text{ MHz} / 60 \text{ MHz}$

In literature a value of $1.685 \cdot 10^{-11}$ m/W for g_B in SMF can be found, as recently reported by Lanticq et al.¹³ The higher g_B for SMF compared to our measured one in PCFs is not contradictive with the higher PCF

nonlinear Kerr coefficient γ . Indeed g_B does not benefit from the smaller PCF effective mode area contrary to the nonlinear Kerr coefficient γ .

The integrated measurement of the Brillouin spectrum motivated us to undertake a distributed measurement of the Brillouin gain as the asymmetry and the stability of the peak indicated already a difference concerning the homogeneity of the fiber.

2.2 Brillouin Threshold

The definition of the Brillouin threshold can be handled in different ways. The theoretical threshold is given by relationship:¹⁴

$$P_{TH} = \frac{21 \cdot K \cdot A_{eff}}{g_B \cdot L_{eff}} \quad (4)$$

where A_{eff} is the effective area of the optical mode, $L_{eff} = \frac{1 - \exp(-\alpha P L)}{\alpha P}$ the effective length and g_B the Brillouin gain. The value of K depends on the fiber type. In a polarization maintaining fiber $K=1$ whereas in a SMF $K=3/2$ as the polarization changes randomly.¹⁵ The Brillouin gain can be determined by measuring the FWHM in the spontaneous Brillouin regime and using Eq. (3). This definition assumes that the threshold is reached when the reflected power equals the transmitted power. For practical reasons, such as a lower input power, it is better to take another definition. Therefore, the threshold is provided where the reflected power is 1% of the injected one.¹⁶ This requires to modify Eq. (4). The numerical factor 21 is approximately the natural logarithm of the gain.¹⁷ Le Floch et al.¹⁸ adjusted this factor depending on the fiber length. For example for 500 m it is equal to 20. Adapting the equation to the 1%-definition changes the numerical factor depending on fiber length and attenuation to 15.5 (#1) and 16 (#2) which is obtained by numerical approximations. With the measured and calculated values the theoretical Brillouin threshold can be estimated at 25.1 dBm (#1) and 20.2 dBm (#2), respectively. The Brillouin threshold is measured with the setup in Fig. 2(a) without the heterodyne detection. Using equation 4 the experimental value of the Brillouin threshold is obtained at 26.7 dBm for fiber #1 and 20.2 dBm for fiber #2 (Fig. 5) with an insertion loss of 1.2-1.5 dB for each splicing. In this figure the backscattered and transmitted power versus the input power is plotted and the threshold is determined graphically. Comparing the theoretical with the experimental values we found them in good accordance for fiber #2. For fiber #1 the experimental value is higher than the theoretical one. This suggests the existence of additional acoustic modes as a higher power is required to bring them to the stimulated regime. Several involved acoustic modes can already be observed when we consider the asymmetric Brillouin spectrum which is due to fiber inhomogeneities. Thus the comparison between the theoretical and experimental value for the Brillouin threshold is another indication for the different fiber homogeneity.

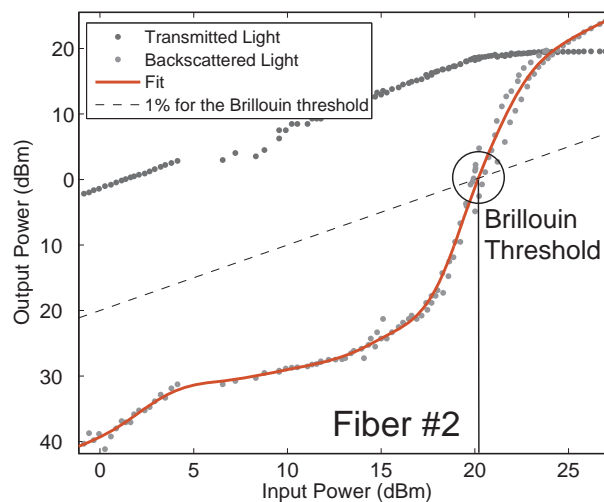


Figure 5. Backscattered and transmitted power versus input power in dBm, fiber #2

2.3 Guided acoustic wave Brillouin scattering

The nature of forward Brillouin scattering, known as GAWBS, is different to backward scattering. The backscattered wave is caused by longitudinal acoustic waves whereas forward Brillouin scattering is induced by transversal acoustic modes.¹⁹ There are radial symmetric modes R_{0M} and torsional-radial modes TR_{2M} , the latter depolarize the pump wave. The GAWBS spectrum in a SMF shows multiple peaks in the region till 1 GHz shifted to the pump wave. This is different for PCF where most of the modes are suppressed apart from one or several main modes.^{20, 21} The reason is the hole structure which makes the fiber core almost independent from the cladding. In this way most of the transversal acoustic modes are disabled contrary to a SMF.

To investigate GAWBS a setup with a fiber loop reflector²² is used as in Fig. 6. In this setup the amplified laser light is injected to the fiber loop reflector via a polarization controller and a 50:50 coupler. The polarization is adjusted to the minimum output power at the other output of the coupler. When GAWBS is not present in the fiber loop, the interference of the counterpropagating light waves at output B is destructive resulting in no signal of the photodiode. Since the transversal elastic modes (GAWBS) induce a phase shift locally in the fiber, we obtain an interference signal in frequency domain. Polarized and depolarized modes are observed with this setup. The polarization is fixed at the input of the photodiode, which is indeed compulsory to select one polarization state only to guarantee a proper interference in the fiber loop reflector.

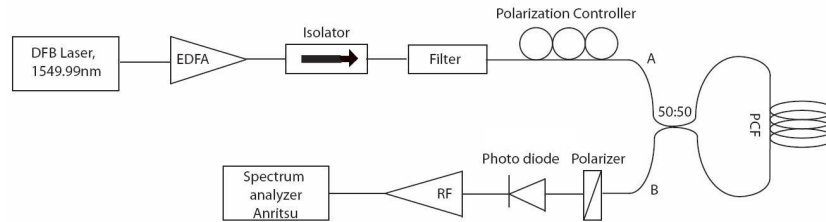


Figure 6. GAWBS measurement setup²¹

The results are presented in Fig. 7. The GAWBS spectra show a peak at 754 ± 2 MHz with a quality factor $* 59 \pm 16$ (#2) and 710 ± 4 MHz with quality factor 12 ± 1 (#1) respectively. The GAWBS spectrum in fiber #1 is less stable, so the averaging smoothes the data curve (Fig. 7(a)). Several modes are involved in the peak broadening and compete simultaneously, which yields the peak instable. The FWHM of fiber #1 is 72 MHz and for fiber #2 12 MHz which causes the distinct difference in the quality factor. Numerical modeling with the finite element method using COMSOL software allows to compute the acousto-optical coefficient which is an indicator of the coupling of the acoustic and optical mode in the fiber core. This coefficient corresponds to the peaks observed in the GAWBS spectrum. Fig. 7(b) shows clearly three main modes at about 771 MHz for fiber #1. Compared to fiber #2 we find that the main peak is narrower and more stable, which is confirmed by the simulation. The mode at 775 MHz is significantly higher compared to the other modes in the low frequency region till 0.4 GHz.

As expected we observed a main peak in the GAWBS spectrum of both fibers which is confirmed by the simulations. Moreover the quality factor and the stability of the peak already suggest at irregularities along the fiber.

The previous experimental results show that the smaller the fiber core the higher the frequency of the main peak.²¹ Indeed, the mode diameter d_m , the transversal acoustic velocity V_T and the frequency of the main peak ν_a are related through:

$$\nu_a = \frac{V_a}{d_m} \quad (5)$$

Using Eq. (5) one can calculate the diameter of the mode at $d_m = 4.24 \mu\text{m}$ (#2) and $d_m = 4.51 \mu\text{m}$ (#1) with $V_T = 3200$ m/s in silica. This can be compared to the values of the effective mode area (EMA) given by the fiber manufacturer in the following table, based on SEM-images:

*Quality factor $Q = \frac{\nu}{\Delta\nu}$

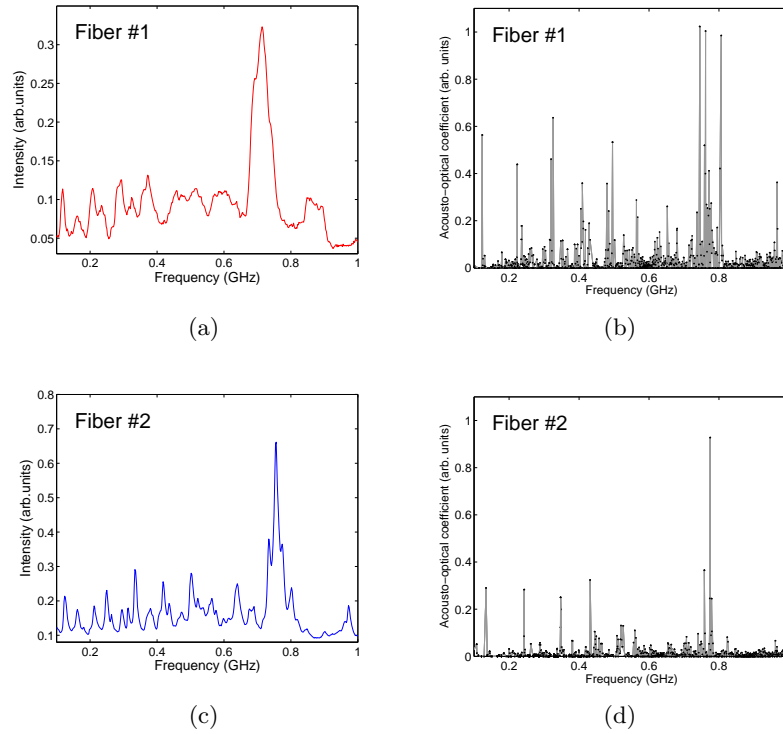


Figure 7. (a),(c) Guided Acoustic Wave Brillouin Scattering (experimental) of fiber #1 and #2, acousto-optical coefficient (simulation) of fiber (b) #1 and (d) #2

Table 3. Values of Effective Mode Area

Fiber	#1	#2
EMA at 1.55 μm by IRCICA (based on SEM-images)	16.1 μm^2	16.9 μm^2
EMA experimental	15.96 \pm 0.19 μm^2	14.15 \pm 0.05 μm^2

For fiber #1 the experimental and numerical results are in good accordance whereas the experimental value for fiber #2 differs from the simulated one.

3. DISTRIBUTED MEASUREMENT

3.1 Distributed Sensing using Brillouin Echoes

In order to map the distributed Brillouin gain of a fiber Brillouin Optical Time Domain Analysis (BOTDA) System has been developed.² It can achieve a spatial resolution till 1 m which is limited by the decay time of the acoustic wave. It was meanwhile advanced to reach a higher resolution: a π phase pump pulse replaces now the intensity pump pulse. A resolution till 5 cm can be achieved, limited by the pulse generator. The experimental setup for Distributed Sensing using Brillouin Echoes (BEDS) is presented in Fig. 8(a). More details can be found in Foaleng et al.²³ The radiation of an external cavity laser diode (1551 nm) is split by a polarization-maintaining coupler. One branch will serve to generate the continuous probe and the other one for the pump pulse. An intensity modulator, driven by a microwave generator, creates two sidebands tuned to the Brillouin frequency of the respective fiber under test (Stokes and Anti-Stokes wave). Only one sideband is used as continuous probe signal.

By adjusting the modulator DC offset it can be driven in a nonlinear regime of its modulation transfer function. In this way the carrier wave is suppressed as much as possible. The probe wave is amplified by an EDFA and injected into the fiber. In the other channel the pump wave is modulated by 3 ns π phase pulses via a phase modulator. 3 ns of the π phase pulse corresponds to 30 cm of spatial resolution in the fiber which is chosen by reason of fiber loss. A polarization controller is used to align the pump and probe polarizations

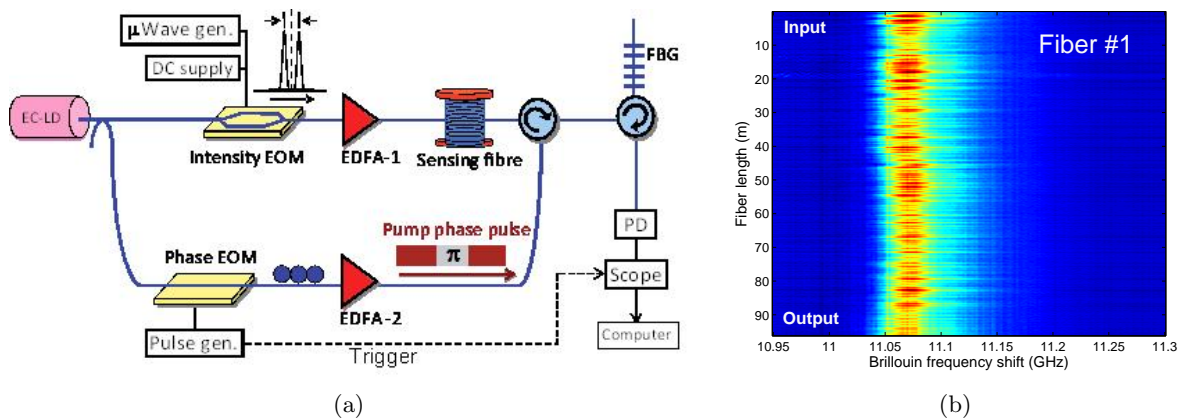


Figure 8. (a) Experimental setup of the optimized BEDS system: EC LD: external cavity laser diode; EDFA: erbium-doped fiber amplifier; EOM: electro-optic modulator; FBG: fiber Bragg grating; PD: photo diode²³ (b) Distributed Brillouin Gain, fiber #1: The curves were fitted by using a convolution with a rectangle to minimize measurement fluctuations

to optimize the acousto-optical interaction before the second EDFA. Passing through an optical circulator the pump pulse is injected into the other end of the fiber under test, so the two signals are counter-propagating. A tunable Fiber Bragg grating connected to a second circulator filters the Stokes-wave and residual pump light. Since the acoustic wave has a finite lifetime (several nanoseconds) the backscattered response continues although the pulse has already left the fiber. This effect is known as second echo.²³ To avoid the undesirable second echo there have been developed two solutions: a numerical technique processing the obtained data and an experimental method by switching off the pump wave after the phase pulse. The latter requires a "double pulse", a pump intensity pulse (about 30 ns) with a π phase pulse (3 ns) at its end.

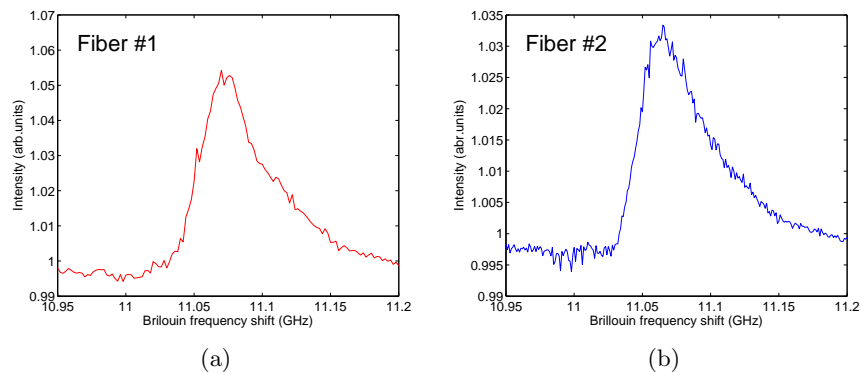


Figure 9. (a), (b) Brillouin gain spectrum at 50m of fiber #1 and #2 respectively

3.2 Results

Besides the integrated measurement of the Brillouin spectrum the distributed one provides further informations concerning inhomogeneities and strain in the fiber. The following data have been obtained with the BEDS-System using the double pulse technique. Fig. 8(b) shows the Brillouin gain along the fiber, obtained by sweeping the modulation frequency. The spatial resolution is 30 cm whereas the resolution of the frequency shift is 2 MHz. Fig. 10(a) and Fig. 10(b) show the longitudinal fluctuations of the Brillouin frequency shift for both fibers. Investigating the distributed Brillouin frequency shift along the 100 m of fiber #1 (Fig. 10(a)) a drop of about 8 MHz can be observed. The main transition is located approximately in the middle of the fiber. This is due to the fiber spooling as the 100 m of the fiber are spooled twofold on half of the fiber coil, so twofold 50 m. The coiling induce strain on the fiber, which changes the frequency shift. This is confirmed by inverting the

fiber (Pump in Input 1 and Pump in Input 2 respectively). Two independent measurements have been taken and the frequency shift behaves in the inverse manner. Thus this long scale fluctuation is not attributed to inhomogeneities in the fiber process. The fast varying irregularities only (about 5 ± 1 MHz every 2 m) can point at a geometric variance of the air-hole structure. This may also be due to the influence of birefringence in the PCF because the order of magnitude is the same. Using Eq. (1) the variation on the refractive index can be calculated to $7 \cdot 10^{-4}$. For comparison the birefringence of PCFs is in general about several 10^{-5} . The distributed BFS of fiber #2 is shown in Fig. 10(b). Between 80 m and 180 m there is a distinct drop of about 5 MHz, which represents exactly one layer of the fiber coil. In this manner we are able to detect the applied strain on one layer whereas the other layers seem not to be affected by strain of the coiling. The short scale fluctuation is smaller (3 ± 1 MHz, every 2-3 m of the fiber) and is due to geometrical changes of the microstructure.

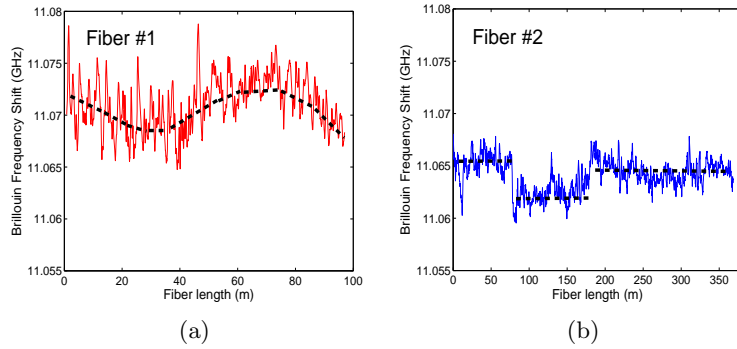


Figure 10. (a), (b) Distributed BFS for fiber #1 and #2 respectively

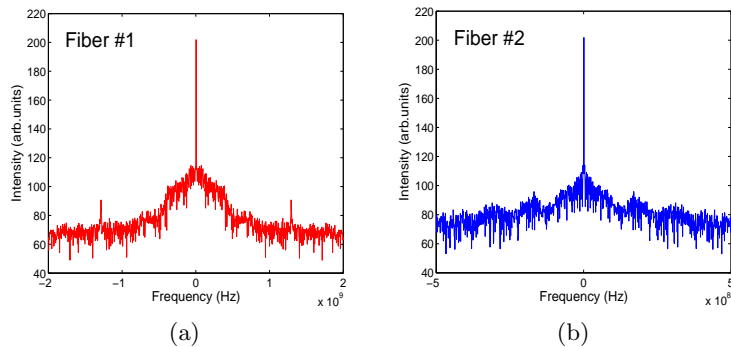


Figure 11. (a), (b) FFT of distributed BFS for fiber #1 and #2 respectively

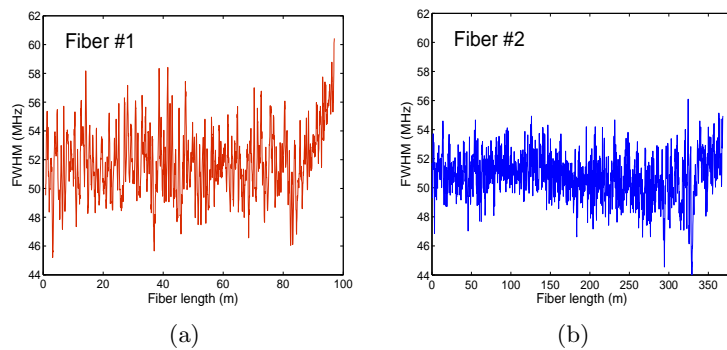


Figure 12. (a), (b) FWHM of distributed Brillouin gain for fiber #1 and #2 respectively

The mean power of the pump pulse in the distributed measurement for both fibers was 13 dBm. Taking into account the splicing losses the pump is assumed to be well below the Brillouin threshold (see chapter 2.2). Comparing our previous measurements of the Brillouin gain spectrum at this power level (about 11.5 dBm) and the spectrum of the distributed measurement at 50 m we find a good agreement for fiber #1 (Fig. 9(a) and Fig. 3(a)). Both spectra are asymmetric which may be explained by several frequency shifted acoustic modes. The peak frequency of the integrated Brillouin spectrum amounts to 11.078 GHz (mean value in the power range 5-28 dBm). The distributed frequency along the fiber is 11.071 ± 0.003 GHz. The same comparison for fiber #2 reveals a discrepancy between the integrated and the distributed measurements (Fig. 9(b) and Fig. 3(b)). The integrated Brillouin gain has a single mode shape but a little bump on the right side can yet be suggested. However the distributed Brillouin spectrum in Fig. 9(b) appears more asymmetric than in the integrated measurement. In the distributed measurement the BFS varies around 11.064 ± 0.002 GHz. The integrated measurement reveals a mean BFS of 11.069 GHz over a power range 3-27 dBm. Nevertheless it is obvious that the fluctuations of the Brillouin shift vary less for fiber #2 as the drawing process was better controlled in order to get a higher homogeneity. The Fourier Transform of the Brillouin shift is shown in Fig. 11(a) and Fig. 11(b). We notice that for fiber #1 the involved frequencies around the main peak are stronger than for fiber #2. This indicates a higher noise and hence confirms our observation. Besides there is a small peak in the frequency spectrum of the distributed Brillouin shift of fiber #1. It corresponds to a regular variation every 16cm along the fiber. A possible explanation is a periodic vibration of the drawing tower during the fabrication process. The analysis of the FWHM of the distributed Brillouin gain is presented in Fig. 12(a) and 12(b). For fiber #1 the distributed FWHM is about 52 ± 2 MHz, compared to 51.5 MHz at 11.5 dBm in the integrated measurement (Fig. 4). The FWHM for fiber #2 is 50 ± 1 MHz (distributed) and 45.4 MHz (integrated). Hence the Brillouin gain broadening for PCF in the spontaneous regime is also noticed in this experiment. Concerning the inhomogeneity we can observe lower fluctuations for fiber #2. In this way the distributed measurement shows the effect of the different drawing process, in terms of the BFS and the FWHM of the Brillouin gain spectrum. Fluctuations in fiber #2 are clearly less pronounced than in fiber #1, as expected.

Table 4. Fluctuations obtained by the distributed measurement

Fiber	#1 - 100 m	#2 - 400 m
BFS (Long scale fluctuations)	11.071 ± 0.003 GHz	11.064 ± 0.002 GHz
Short scale fluctuations	4-6 MHz	3-4 MHz
FWHM	52 ± 2 MHz	50 ± 1 MHz

The distributed measurement reveals a detailed mapping of the BFS along the fiber. Our aim is to link the variation of the BFS to geometrical irregularities along the fiber. By using Eq. (1) we can obtain the distributed effective refractive index n_{eff} dependent on the BFS. To relate geometrical variations to n_{eff} the dependency of n_{eff} on the structure scale has been simulated by using the cross section of both fibers via Comsol (Fig. 13). A simulation based on the original SEM-image (corresponding to 100% in Fig. 13) leads to a certain value of n_{eff} (1.434 for #2 and 1.432 for #1). By varying the scale of the original SEM-image different values for n_{eff} are obtained and depicted in Fig. 13 for the two PCFs.

We then computed the local derivation of the obtained relation between n_{eff} and the geometrical scale around the 100% - value, e.g. the original SEM-image. This is compared to the fluctuations of the effective refractive index in the fibers under test by using Eq. (1). The long scale variations are due to fiber coiling induced stress whereas the short scale fluctuation can point at drawing induced geometrical variations. The standard deviation of these short scale fluctuations are $2.6 \cdot 10^{-4}$ (#1) and $1.0 \cdot 10^{-4}$ (#2) which correspond to 1.3% and 0.5% of scale variation. The peak-to-peak variation is 7% (#1) and 3% (#2). Since polarization and strain can influence the variation of the effective refractive index the contribution of the structure size should be even below these values. This confirms the higher quality of the drawing process of fiber #2. For comparison some manufacturers like Crystal Fibre promote their fibers with a variation of 4% (fiber core $2.4 \pm 0.1 \mu\text{m}$)²⁴ and Euser et al.²⁵ indicates to produce fibres with a precision of 2%. Our results demonstrate the ability of the high precision distributed measurement to distinguish both qualitatively and quantitatively between different drawing processes.

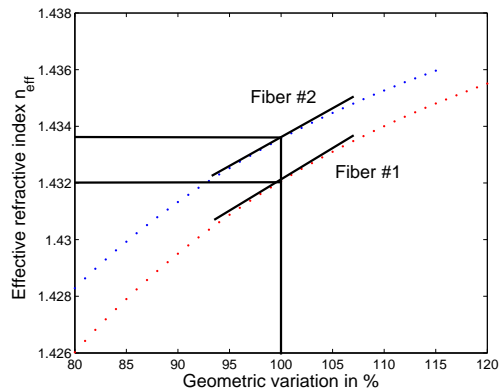


Figure 13. Variation of the effective refractive index while tuning the scale of the SEM-image

4. CONCLUSION

The homogeneity of two photonic crystal fibers drawn from the same preform but with a different drawing process has been investigated. The integrated measurement included the studies of the backscattered Brillouin gain spectrum, the Brillouin threshold and guided acoustic wave Brillouin scattering, where we found indications for the differently pronounced homogeneity of the fibers. Besides guided acoustic wave Brillouin scattering enabled us to estimate the effective mode area of photonic crystal fibers. The results of the integrated experiments has been confirmed by our distributed measurement of the backscattered Brillouin gain. The variation of the Brillouin frequency shift as well as the distributed Full Width at Half Maximum was less distinct in case of the fiber with the better controlled drawing process. The exploitation of the Brillouin frequency shift could be used to evaluate geometric variations of the fiber. Hence it has been shown that a complete investigation of Brillouin scattering reveals quantitative informations not only about the applied strain but also about the quality of the drawing process.

ACKNOWLEDGMENTS

We thank the COST299 Action for financial support and V. Laude for helpful discussions. This work was funded by the European Interreg IV A program and the Fond Européen de Développement Régional (FEDER).

REFERENCES

- [1] Ippen, E. and Stolen, R., "Stimulated Brillouin scattering in optical fibers," *Applied Physics Letters* **21**(11), 539–541 (1972).
- [2] Niklès, M., Thévenaz, L., and Robert, P. A., "Simple distributed fiber sensor based on Brillouin gain spectrum analysis," *Optics Letters* **21**(10), 758–760 (1996).
- [3] Zou, L., Bao, X., and Chen, L., "Distributed Brillouin temperature sensing in photonic crystal fiber," *Smart Materials and Structures* **14**(3), S8 (2005).
- [4] Dainese, P., Russell, P. S. J., Joly, N., Knight, J. C., Wiederhecker, G. S., Fragnito, H. L., Laude, V., and Khelif, A., "Stimulated Brillouin scattering from multi-GHz-guided acoustic phonons in nanostructured photonic crystal fibres," *Nature Physics* **2**(6), 388–392 (2006).
- [5] Minardo, A., Bernini, R., Urbanczyk, W., Wojcik, J., Gorbatov, N., Tur, M., and Zeni, L., "Stimulated Brillouin scattering in highly birefringent microstructure fiber: experimental analysis," *Optics Letters* **33**, 2329–2331 (OCT 15 2008).
- [6] Beugnot, J.-C., Sylvestre, T., Alasia, D., Maillotte, H., Laude, V., Monteville, A., Provino, L., Traynor, N., Foalet Mafang, S., and Thévenaz, L., "Complete experimental characterization of stimulated Brillouin scattering in photonic crystal fiber," *Optics Express* **15**(23), 15517–15522 (2007).

- [7] Niklès, M., Thévenaz, L., and Robert, P. A., “Brillouin gain Spectrum Characterization in Single-Mode Optical Fiber,” *Journal of Lightwave Technology* **15**(10), 1842–1851 (1997).
- [8] Malitson, I., “Interspecimen comparison of refractive index of fused silica,” *Journal of the optical society of America* **54**(11), 1401 (1964).
- [9] Gaeta, A. L. and Boyd, R., “Stochastic dynamics of Stimulated Brillouin Scattering in an optical fibers,” *Physical Review A* **44**(5), 3205–3208 (1991).
- [10] Yeniay, A., Delavaux, J. M., and Toulouse, J., “Spontaneous and Stimulated Brillouin Scattering Gain Spectra in Optical Fibers,” *Journal of Lightwave Technology* **20**(8), 1425 (2002).
- [11] Floch, S. L. and Cambon, P., “Study of Brillouin gain spectrum in standard single-mode optical fiber at low temperatures (1.4370 K) and high hydrostatic pressures (1250 bars),” *Optics Communications* **219**, 395–410 (2003).
- [12] Lanticq, V., Jiang, S., Gabet, R., Jaoun, Y., Taillade, F., Moreau, G., and Agrawal, G. P., “Self-referenced and single-ended method to measure Brillouin gain in monomode optical fibers,” *Optics Letters* **34**, 1018–1020 (2009).
- [13] Agrawal, P., [*Nonlinear Fiber Optics*], Academic Press, third ed. (2001).
- [14] Deventer, M. O. V. and Boot, A. J., “Polarisation properties of Stimulated Brillouin Scattering in Single Mode Fibers,” *Journal of Lightwave Technology* **12**(4), 585–590 (1994).
- [15] Boyd, R., Rzazewski, K., and Narum, P., “Noise initiation of Stimulated Brillouin Scattering,” *Physical Review A* **42**(9), 5514–5521 (1990).
- [16] Smith, R. G., “Optical power handling capacity of low loss optical fibers as determined by Stimulated Raman and Brillouin Scattering,” *Applied Optics* **11**(11), 2489 (1972).
- [17] Floch, S. L. and Cambon, P., “Theoretical evaluation of the Brillouin threshold and steady-state Brillouin equations in standard single-mode optical fibers,” *Journal of the optical society of America A* **20**(6), 1132–1137 (2003).
- [18] Shelby, R., Levenson, M., and Bayer, P., “Resolved forward Brillouin scattering in optical fibers,” *Physical Review Letters* **54**, 939–942 (1985).
- [19] Elser, D., Andersen, U. L., Korn, A., Glockl, O., Lorenz, S., Marquardt, C., and Leuchs, G., “Reduction of Guided Acoustic Wave Brillouin Scattering in Photonic Crystal Fibers,” *Physical Review Letters* **97**, 133901 (2005).
- [20] Beugnot, J.-C., Sylvestre, T., Maillotte, H., Mélin, G., and Laude, V., “Guided acoustic wave Brillouin scattering in photonic crystal fibers,” *Optics Letters* **32**(1), 17–19 (2006).
- [21] Mortimore, D., “Fiber loop reflectors,” *Journal of Lightwave Technology* **6**(7), 1217–1224 (1988).
- [22] Foaleng Mafang, S., Beugnot, J.-C., and Thévenaz, L., “Optimized configurarion for high resolution distributed sensing using Brillouin echoes,” *75032C(7503)*, Proceedings SPIE, UK, Edinburgh (2009).
- [23] Crystal Fibres, Characteristics of product, <http://www.nktphotonics.com/files/files/NL-24-800.pdf>.
- [24] Euser, T. G., Chen, J. S. Y., Scharrer, M., Russell, P. S. J., Farrer, N. J., and Sadler, P. J., “Quantitative broadband chemical sensing in air-suspended solid-core fibers,” *Journal of Applied Physics* **103**, 103108 (2008).